

---

# Resilience of Bayesian Layer-Wise Explanations under Adversarial Attacks

---

**Ginevra Carbone**

Department of Mathematics and Geosciences  
University of Trieste, Trieste, Italy  
ginevra.carbone@phd.units.it

**Luca Bortolussi**

Department of Mathematics and Geosciences  
University of Trieste, Trieste, Italy;  
Modeling and Simulation Group,  
Saarland University, Saarland, Germany  
luca.bortolussi@gmail.com

**Guido Sanguinetti**

School of Informatics, University  
of Edinburgh, Edinburgh, United Kingdom;  
SISSA, Trieste, Italy  
gsanguin@inf.ed.ac.uk

## Abstract

We consider the problem of the stability of saliency-based explanations of Neural Network predictions under adversarial attacks in a classification task. Saliency interpretations of deterministic Neural Networks are remarkably brittle *even when the attacks fail*, i.e. for attacks that do not change the classification label. We empirically show that interpretations provided by Bayesian Neural Networks are considerably more stable under adversarial perturbations. By leveraging recent results, we also provide a theoretical explanation of this result in terms of the geometry of adversarial attacks. Additionally, we discuss the stability of the interpretations of high level representations of the inputs in the internal layers of a Network. Our results not only confirm that Bayesian Neural Networks are more robust to adversarial attacks, but also demonstrate that Bayesian methods have the potential to provide more stable and interpretable assessments of Neural Network predictions.

## 1 Introduction

Deep Neural Networks (DNNs) are the core engine of the modern AI revolution. Their universal approximation capabilities, coupled with advances in hardware and training algorithm, have resulted in remarkably strong predictive performance on a variety of applications, from computer vision to natural language to bioinformatics.

While the story of DNNs is indubitably one of success, it is tempered with a number of potentially very serious drawbacks which are somehow the natural flip side of dealing with extremely flexible and complex models. The first such drawback is the black box nature of DNNs: their expressivity and training on large data sets empirically results in very strong predictive power, but in general it does not provide any intuition about the possible explanations underlying the decisions. The opaqueness of DNNs decisions is a major hurdle towards their usage in scientific applications, where frequently explanations for decisions are even more important than accuracy. It is even more problematic in many societal applications, where several countries mandate by law the explainability of any algorithmic decision in a variety of contexts.

A second major drawback of DNN predictions is their vulnerability to adversarial attacks: empirically, it has been observed in many applications that well chosen infinitesimal changes in inputs can produce catastrophic changes in output [11], leading to paradoxical classifications and a clear problem in any application to safety critical systems. Such brittleness appears to be intimately related to the geometry of the data itself [5], and is therefore likely to be an intrinsic feature of standard DNN predictions.

In this paper, we argue theoretically and empirically<sup>1</sup> that these two problems are interlinked, and that therefore solutions that ameliorate resilience against adversarial attacks will also lead to more stable and reliable interpretations. We work within the framework of (pixel-wise) saliency explanations, which attempt to interpret post-hoc DNN decisions by apportioning a relevance score to each input feature for each data point. Specifically, we use the popular Layer-wise Relevance Propagation (LRP) [3], a method to assess the contribution of each pixel to the final classification score which backpropagates the prediction in the neural network until it reaches the input, using a set of suitable propagation rules. LRP saliency interpretations are well known to be unstable under perturbations of the inputs [10, 13, 1, 28]; recently, [4] suggested that a Bayesian treatment might ameliorate these stability problems.

Here, we consider the stability of saliency interpretations under targeted adversarial attacks that aim to change the classification under perturbations of the input. We introduce a novel notion of LRP robustness under adversarial attacks. As previously observed in [10, 12, 7], our results confirm that the LRP robustness of deterministic DNN predictions is remarkably low even when the adversarial attack fail to change the overall classification of the data point, i.e. that LRP interpretations are *less robust* than actual classifications. Considerations on the geometry of LRP [2] suggest that the observed lack of robustness might be imputable to large gradients of the prediction function in directions orthogonal to the data manifold. Here we expand on such a point of view, integrating it with a theoretical analysis in a suitably defined large-data limit [5, 23, 8, 19], and leveraging recent results from [5] about the robustness of BNNs to gradient based adversarial attacks. Specifically, we prove that Bayesian training of the DNNs in the large-data and overparametrized limit induces a regularizing effect which naturally builds robust explanations. We empirically validate this claim on the popular MNIST and Fashion MNIST benchmarks.

The main contributions of this paper are:

1. The definition of a novel metric of robustness of interpretations of DNN results (Sec. 3.1);
2. A theoretical analysis of the effects of adversarial attacks on prediction interpretations, and of the improvements offered by a Bayesian treatment (Sec. 3.2);
3. An empirical study showing that indeed Bayesian training and prediction leads to more robust interpretations of classifications (Sec. 4).

## 2 Background

### 2.1 Layer-Wise Relevance Propagation

Let  $f : \mathbb{R}^d \rightarrow [0, 1]$  be a single-class image classifier, where  $f(x, w)$  is the probability that an image  $x \in \mathbb{R}^d$  belongs to the class of interest and  $w$  is the set of learnable weights. Without loss of generality, this concept can be extended to multi-class classifiers or to non probabilistic outputs. The idea of pixel-wise decomposition of a given image  $x$  is to understand how its pixels contribute to the prediction  $f(x, w)$ . In particular, LRP associates with each pixel  $p$  a relevance score  $R(x_p, w)$ , which is positive when the pixel contributes positively to the classification, negative when it contributes negatively to the classification and zero when it has no impact on the classification. All the relevance scores for a given image  $x$  can be stored in a heatmap  $R(x, w) = \{R(x_p, w)\}_p$ , whose values quantitatively explain not only whether pixels contribute to the decision, but also by which extent. By leveraging suitable propagation rules, one can ensure that relevance heatmap catch saliency features. For this purpose, the heatmap should be *conservative*, i.e. the sum of the assigned relevances should correspond to the total relevance detected by the model

$$f(x, w) = \sum_p R(x_p, w).$$

---

<sup>1</sup>Code is available at <https://github.com/ginevracoal/BayesianRelevance>.

Several propagation rules satisfy the conservative property, each of them leading to different relevance measures. In Sec. A.2 of the supplementary material we report three practical propagation rules: the Epsilon rule, the Gamma rule and the Alpha-Beta rule. [3] also presented LRP using a functional approach, i.e. independently of the network’s topology. Then, [21] used *deep Taylor decomposition* to express any rule-based approach under the functional setting. Their method builds on the standard first-order Taylor expansion of a non-linear classifier at a chosen *root point*  $x^*$ , such that  $f(x^*) = 0$ ,

$$\begin{aligned} f(x) &= f(x^*) + \nabla_x f(x^*) \cdot (x - x^*) + \gamma \\ &= \sum_p \frac{\partial f}{\partial x_p} \Big|_{x=x^*} \cdot (x_p - x_p^*) + \gamma, \end{aligned} \quad (1)$$

where  $\gamma$  denotes higher-order terms. The root point  $x^*$  represents a neutral image which is similar to  $x$ , but does not influence classification, i.e. whose relevance is everywhere null. The nearest root point to the original image  $x$  can be obtained by solving an iterative minimization problem [21]. The resulting LRP heatmap is  $R(x) = \nabla_x f(x^*, w) \cdot (x - x^*)$ .

## 2.2 Adversarial Attacks

Adversarial attacks are small perturbations of input data that lead to large changes in output (in the classification case, changes in predicted label) [11]. Broadly speaking, most attack strategies utilise information on the DNN loss function to detect an optimal perturbation direction, either through explicit knowledge of the loss function (*white box attacks*) or via querying the DNN (*black box attacks*, generally weaker than their white box counterpart).

White box attacks generally utilize gradient information on the loss function to determine the attack direction. One of the best known gradient-based attacks is the Fast Gradient Sign Method (FGSM) [11], a one-step untargeted attack (i.e., an attack strategy which is independent of the class of the attacked point). For a given network  $f(\cdot, w)$  it crafts a perturbation in the direction of the greatest loss w.r.t. the input

$$\tilde{x} = x + \delta \operatorname{sgn} \nabla_x L(x, w),$$

where  $L$  is the training loss and  $\delta$  is the perturbation magnitude (*strength* of the attack). An iterative, improved version of FGSM is Projected Gradient Descent (PGD) [16]. PGD starts from a random perturbation in an  $\epsilon$ - $L_\infty$  ball around the input sample. At each step, it performs FGSM with a smaller step size,  $\alpha < \epsilon$ , and projects the adversary back in the  $\epsilon$ - $L_\infty$  ball

$$x_{t+1} = \operatorname{Proj}\{x_t + \alpha \cdot \operatorname{sgn} \nabla_x L(x_t, w)\}.$$

The size of the resulting perturbation is smaller than  $\epsilon$ .

The evaluation of adversarial attacks can be either qualitative or quantitative. In the qualitative case, one simply observes whether an attack strategy with a certain strength is successful in switching the classification label of the given data point; in general, the evaluation then reports the fraction of successful attacks on the whole data set. A quantitative metric to evaluate network performances against adversarial attacks is provided by the notion of *softmax robustness* [5], which computes the softmax difference between original and adversarial predictions

$$1 - \|f(x) - f(\tilde{x})\|_\infty. \quad (2)$$

and is a number between zero (maximal fragility) and one (complete robustness) for every data point.

### 2.3 Bayesian Neural Networks

Bayesian models capture the inherent uncertainty intrinsic in any model by replacing individual models with ensembles weighted by probability laws. In the DNN setup, a Bayesian Neural Network (BNN) consists of an ensemble of DNNs whose weights are drawn from the posterior measure  $p(w|D)$ , where  $D$  denotes the available training data. To compute the posterior measure, one needs to first define a prior distribution  $p(w)$  on the network's weights  $w$ ; by Bayes' theorem, the posterior is then obtained by combining the prior and the likelihood  $p(w|D) \propto p(D|w)p(w)$ , where the likelihood term  $p(D|w)$  quantifies the fit of the network with weights  $w$  to the available training data. Exact computation of the posterior distribution  $p(w|D)$  is in general infeasible, thus one needs to resort to approximate inference methods for training Bayesian NNs, namely Hamiltonian Monte Carlo (HMC) [22] and Variational Inference (VI) [25].

Once the posterior distribution has been computed, BNNs produce predictions through the *posterior predictive distribution*

$$p(f(x)|D) = \int dw p(f(x)|w)p(w|D) \simeq \sum_{w_j \sim p(w|D)} p(f(x)|w_j), \quad (3)$$

where  $f(x)$  is the output value at a new point  $x$  and the equality represents the celebrated *Bayesian model averaging* procedure.

In the BNN setting, adversarial attacks are crafted against the posterior predictive distribution  $p(f(x)|D)$ . For example, FGSM attack on an ensemble of  $N$  networks  $f(\cdot, w_i)$  with weights drawn from  $p(w|D)$  becomes

$$\begin{aligned} \tilde{x} &= x + \delta \operatorname{sgn} \left( \mathbb{E}_{p(w|D)} [\nabla_x L(x, w)] \right) \\ &\simeq x + \delta \operatorname{sgn} \sum_{i=1}^N \nabla_x L(x, w_i) \quad w_i \sim p(w|D). \end{aligned}$$

In a similar way, it is possible to introduce a concept of *Bayesian explanations* for BNN predictions. As is clear from the definition(s) of LRP in Section 2.1, the relevance score assigned to an input feature depends on the neural network weights. Therefore, in the Bayesian setting, the relevance becomes a random variable; we define as a Bayesian explanation the expected relevance of a feature under the posterior distribution of the weights.

Recent research shows that Bayesian neural networks are adversarially robust to gradient-based attacks in the over-parametrised and infinite data limit [5, 23]. It is therefore of interest to investigate whether such robustness also extends to the learned explanations. To do so, we compare the explanations of deterministic NNs to that of Bayesian NNs against such attacks. Fig. 1 shows an example of failed FGSM attack for a deterministic network and a Bayesian network with the same architecture. Despite the fact that the attack did not manage to change the overall classification, we can see immediately a large difference between the deterministic LRP explanation of the original image,  $R(x)$ , and of the adversarial image,  $R(\tilde{x})$  (top row). On the other hand, in the Bayesian case (bottom row), the saliency maps before and after the attack are essentially identical. In the next sections, we will provide both a theoretical explanation of this phenomenon, and systematically substantiate empirically the robustness of Bayesian explanations to adversarial attacks.

## 3 Methodology

### 3.1 LRP Robustness

We define the  *$k$ -LRP robustness* of relevance heatmaps to adversarial attacks and use this measure to assess how adversarial perturbations affect the explanations.

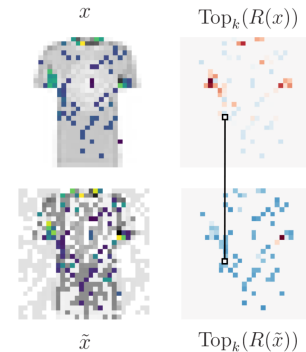


Figure 2: Top<sub>200</sub> pixels in an image  $x$  from Fashion MNIST dataset and an FGSM adversarial perturbation  $\tilde{x}$ .

**Definition 3.1.** Let  $x$  be an image with relevance heatmap  $R(x, w)$  and  $\tilde{x}$  an adversarial perturbation with relevance heatmap  $R(\tilde{x}, w)$ . Let  $\text{Top}_k(R)$  denote the set of  $k$  most relevant pixel indexes in a heatmap  $R$ , where  $P \in \mathbb{N}$  is the total number of pixels in  $x$  and  $k \leq P$ . The  $k$ -LRP robustness of  $x$  w.r.t. the attack  $\tilde{x}$  is

$$k\text{-LRP}_\rho(x, \tilde{x}, w) := \frac{|\text{Top}_k(R(x, w)) \cap \text{Top}_k(R(\tilde{x}, w))|}{k}. \quad (4)$$

In other words,  $k\text{-LRP}_\rho(x, \tilde{x}, w)$  is the fraction of common  $k$  most relevant pixels for  $x$  and  $\tilde{x}$ . Fig. 2 gives an intuition of this computation. Notice that the LRP robustness of a point depends only implicitly on the strength of the attack through the attacked point  $\tilde{x}$ .

### Inner layers explanations

We analyse the behaviour of LRP representations in the internal layers of the network, thus we also extend the computation of LRP heatmaps to any feature representation of the input  $x$  at a learnable layer  $l \in \mathbb{N}$ . We denote it by  $R(x, w, l)$ , where  $l \leq L$  and  $L$  is the maximum number of layers available in the architecture. The corresponding LRP robustness will be denoted by  $k\text{-LRP}_\rho(x, \tilde{x}, w, l)$ . In such case, the robustness does not refer anymore to explanations in the classification phase (pre-softmax layer), but rather to the explanations in the learning phases, hence it gives an idea of the most relevant pixels determining an internal representation.

Fig. 3 shows an example of internal LRP heatmaps on a deterministic NN with learnable layers indexed by  $l \in [0, 3, 7]$ . For illustrative purposes, heatmaps appearing on the same row are normalized in  $[-1, 1]$  before selecting the  $\text{Top}_k$  pixels, since numeric scales are significantly different across the different internal representations.

**Bayesian LRP robustness** The notion of LRP robustness can be naturally generalised to the Bayesian setting using the concept of Bayesian model averaging introduced in Section 2.3. Hence, the LRP heatmap of a BNN is computed as the average of all the deterministic heatmaps from the ensemble:

$$\mathbb{E}_{p(w|D)}[k\text{-LRP}_\rho(x, \tilde{x}, w, l)].$$

In this regard, we emphasise that Bayesian interpretations are affected by the chosen number of posterior samples drawn from the learned distribution.

### 3.2 Geometric meaning of adversarial interpretations

To better conceptualise the impact of a Bayesian treatment on LRP robustness, it is convenient to consider the thermodynamic limit of infinite data and infinite expressivity of the network, as formalised in [8, 19, 23]. For the purposes of our discussion, the main ingredients are the data manifold  $\mathcal{M}_D$ , a piecewise smooth submanifold of the input space where the data lie, and the true input/output function, which is assumed to be smooth and hence representable through an infinitely wide DNN. Practically, this limit might be well approximated on large data sets where the networks achieve high accuracy.

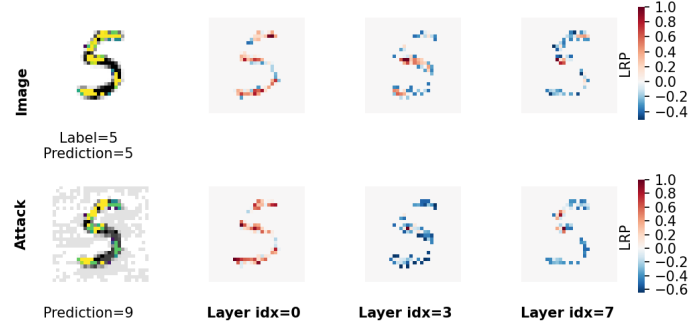


Figure 3: LRP heatmaps of an image  $x$  and an FGSM adversarial perturbation  $\tilde{x}$ . Explanations are computed using the Epsilon rule w.r.t. the learnable layers of a deterministic network trained on the MNIST dataset. For each layer, we only show the 100 most relevant pixels for both the original image and its adversarial counterpart, i.e. the ones selected for the computation of  $100\text{-LRP}_\rho(x, \tilde{x}, w, l)$  from Eq. (4), where  $l \in [0, 3, 7]$ .

In this limit, it was proved in [8, 19, 23] that the DNN  $f(x, w)$  trained via SGD will converge to the true underlying function  $g(x)$  over the whole data manifold  $\mathcal{M}_D$ . Because the data manifold is assumed to be piecewise smooth, it is possible to define a tangent space to the data manifold almost everywhere, and therefore to define two operators  $\nabla_x^\perp$  and  $\nabla_x^\parallel$  which define the gradient along the normal and tangent directions to the data manifold  $\mathcal{M}_D$  at a point  $x$  of a function defined over the whole input space.

LRP and gradient-based adversarial strategies both share a reliance on gradient information. In the adversarial attacks cases, one evaluates the gradient of the loss function which, by the chain rule is given by

$$\nabla_x L(f, g) = \frac{\delta L(f, g)}{\delta f} \frac{\partial f}{\partial x} \quad (5)$$

In the thermodynamic limit, the DNN function  $f(x, w)$  coincides with the true function everywhere on the data manifold, and therefore the tangent gradient of the loss function is identically zero. The normal gradient of the loss, however, is unconstrained by the data, and, particularly in a high dimensional setting, might achieve very high values along certain directions, creating therefore weaknesses that may be exploited by an adversarial attacker. The main result of [5] was to show that the orthogonal component of the loss gradient has expectation zero under the posterior weight distribution, therefore showing that BNNs are robust against adversarial attacks.

In the LRP setup, we instead consider gradients of the prediction function, as opposed to the loss, nevertheless the insight remains valid. The tangent components of the gradient of the prediction function  $f(x, w)$  will coincide with the gradients of the true function  $g(x)$ , and therefore represent directions of true sensitivity of the decision function which are correctly recognised as relevant. However, such directions might be confounded or dwarfed by normal gradient components, which create directions of apparent relevance which, by construction, are targeted by gradient-based adversarial attacks. In Theorem 3.1 we prove that BNNs in the thermodynamic limit will only retain relevant directions along the data manifold, which correspond to genuine directions of high relevance.

**Theorem 3.1.** *Let  $\mathcal{M}_D \subset \mathbb{R}^d$  be an a.e. smooth data manifold and let  $f(x, w)$  be an infinitely wide Bayesian neural network, trained on  $\mathcal{M}_D$  and at full convergence of the training algorithm. Let  $p(w|D)$  be the posterior weight distribution and suppose that the prior distribution  $p(w)$  is uninformative. In the limit of infinite training data, for any  $x \in \mathcal{M}_D$ ,*

$$\mathbb{E}_{p(w|D)}[\nabla_x^\perp f(x, w)] = 0.$$

Therefore, the orthogonal component of the gradient of the prediction function vanishes in expectation under the posterior weight distribution and Bayesian averaging of the relevance heatmaps naturally builds explanations in the tangent space  $T_x \mathcal{M}_D$ . Specifically, from the deep Taylor decomposition on a root point  $x^* \in \mathcal{M}_D$  we obtain the expected LRP heatmap

$$\mathbb{E}_{p(w|D)}[R(x)] = \mathbb{E}_{p(w|D)}[\nabla_x f(x^*, w)] \cdot (x - x^*) = \mathbb{E}_{p(w|D)}[\nabla_x^\parallel f(x^*, w)] \cdot (x - x^*).$$

We refer the reader to Sec. A.1 of the Appendix for the theoretical background material and for a formal proof of Theorem 3.1.

It should be noticed that LRP heatmaps at layer  $l$  involve partial derivatives w.r.t.  $x$  of the subnetwork  $f^l(\cdot, w)$  of  $f$ , which associates to an input  $x$  the  $l$ -th activation from  $f(\cdot, w)$ . Consequently, the same vanishing property of the gradients holds for explanations in the internal layers - which are therefore more robust in the Bayesian case.

## 4 Experimental Results

In this section we corroborate the insights described in Section 3 with an experimental evaluation, comparing empirically the LRP robustness using the popular MNIST [17] and Fashion MNIST [27] benchmark data sets. Both data sets are composed of 60.000 images belonging to ten classes: in the MNIST case, these are hand-written digits, while the Fashion MNIST data set consists of stylized Zalando images of clothing items. While MNIST is considered a relatively trivial data set, with accuracies over 99% being regularly reported, Fashion MNIST is considerably more complex, and the best architectures report accuracies around 95%. We do not experiment on more complex data sets such as CIFAR-10 [15] or ImageNet [6], because of the very high computational costs of running

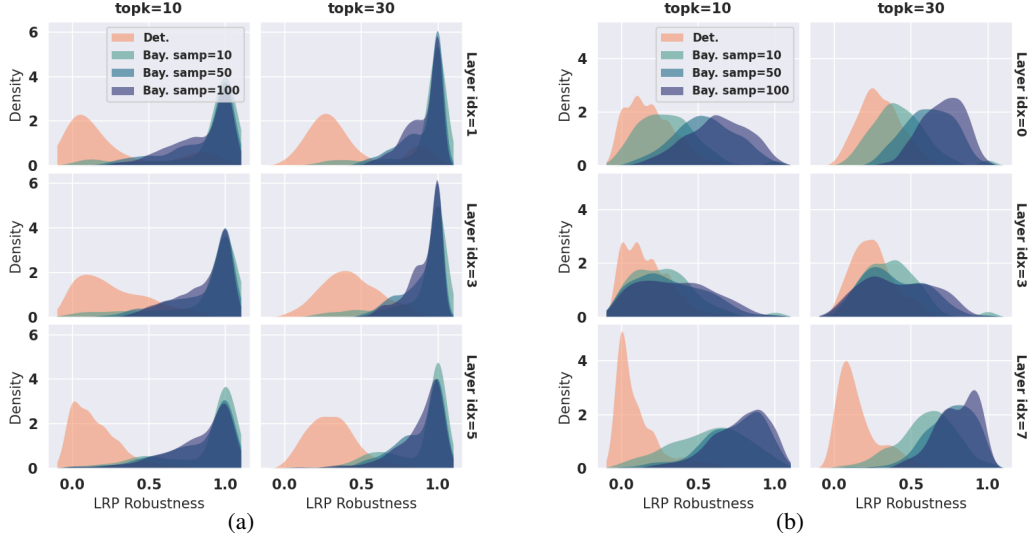


Figure 4: LRP robustness distributions for FGSM attacks computed on 500 test points from MNIST (a) and Fashion MNIST (b) datasets, using the Epsilon rule. Networks in (a) have a fully connected architecture (Tab. 2 in the Appendix) and are trained with HMC. Networks in (b) have a convolutional architecture (Tab. 1 in the Appendix) and are trained with VI. Bayesian networks are tested with an increasing number of samples (10, 50, 100). Layer indexes refer to the learnable layers in the architectures.

Bayesian inference on very deep networks trained on very large data sets <sup>2</sup>. Simulations were conducted on a machine with 36 cores, Intel(R) Xeon(R) Gold 6140 CPU @ 2.30GHz processors and 192GB of RAM.

On both data sets, we train deterministic DNNs and BNNs using both HMC and VI: this allows us to contrast the effect of a locally Gaussian approximation to the posterior against the asymptotically exact (but computationally more expensive) approximation provided by HMC. Because we require high accuracy in order to approximate the asymptotic conditions described in Section 3.2, different architectures were used on the two data sets and between VI and HMC. In all cases, however, the BNN is compared with a DNN with the same architecture, to ensure fairness of the comparisons. Full details of the architectures used are reported in Sec. A.3 of the Appendix.

Adversarial attacks in our tests are Fast Gradient Sign Method (FGSM) [11] and Projected Gradient Descent (PGD) [16], with a maximum perturbation size of 0.25. We rely on *TorchLRP* library <sup>3</sup> for the computation of the LRP explanations and set  $\epsilon = 0.1$  in the Epsilon rule,  $\gamma = 0.1$  in the Gamma rule,  $\alpha = 1$ ,  $\beta = 0$  in the Alpha-Beta rule.

#### 4.1 Bayesian interpretations are robust against the attacks

Our first significant result is that Bayesian explanations are considerably more robust under attacks than deterministic architectures. For both data sets and both VI and HMC training, LRP robustness scores are significantly higher than their deterministic counterparts. These results are shown for MNIST and Fashion MNIST data sets using the Epsilon rule and VI and HMC training in Fig. 4 and Fig. 7 in the Appendix. The last row of the figures represents the standard LRP (computed from the pre-softmax layer), while the top row is the initial feature representation (after the first non-linear layer), and the middle row represents the LRP of an internal layer. We tested Bayesian representations using an increasing number of posterior samples, i.e. 10, 50, 100 and two different choices of  $k$ ,  $k = 10$  and  $k = 30$  (columns). We attacked 500 randomly selected test images, whose choice is balanced w.r.t. the available classes, and plot the distribution of the resulting LRP scores.

<sup>2</sup>We do not experiment with scalable Monte Carlo dropout methods [9] here since there is no guarantee that their uncertainty estimates are able to capture the full posterior [24].

<sup>3</sup><https://github.com/fhvilsthoj/TorchLRP>

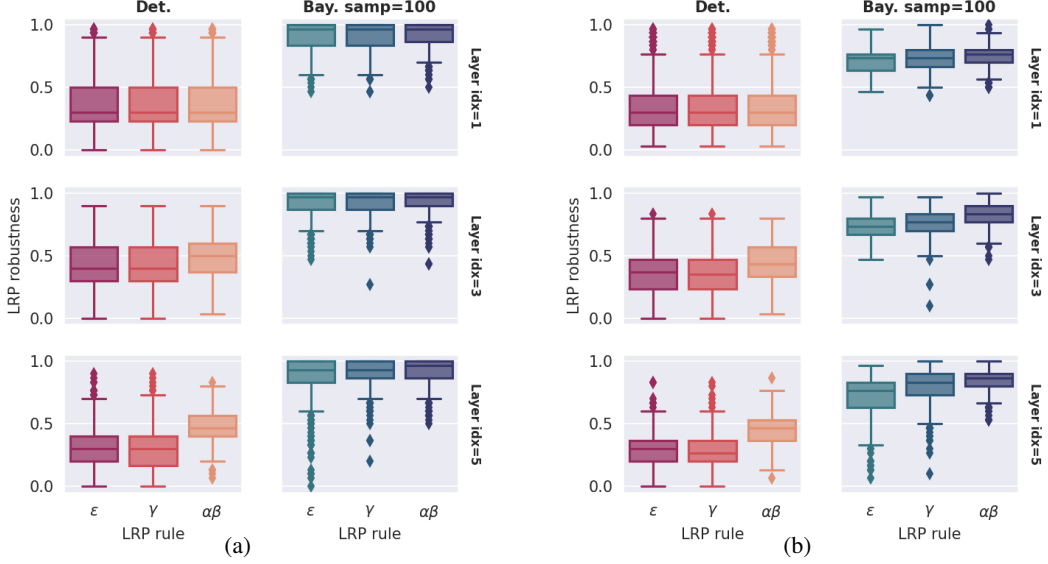


Figure 5: LRP robustness for FGSM (a) and PGD (b) attacks computed on 500 test points from MNIST dataset using Epsilon, Gamma and Alpha-Beta rules on the Top<sub>30</sub> pixels. Deterministic and Bayesian networks have the same fully connected architecture (Tab. 2) and are trained with HMC. Layer indexes refer to the learnable layers in the architecture. Bayesian networks are tested with 100 posterior samples. The parameters are set to:  $\epsilon = 0.1$ ,  $\gamma = 0.1$ ,  $\alpha = 1$ ,  $\beta = 0$ .

The first notable observation is that in both data sets and with both inference method the Bayesian (pre-softmax) LRP has robustness values very close to one. Interestingly, the behaviour of the LRP in the inner layers appears to be rather different between VI and HMC: while HMC seems stable across all layers, networks trained with VI appear to have a broadening of the LRP distribution in the intermediate layers, suggesting that compensatory changes happen between the early and late layers. Importantly, we see that deterministic DNNs have very low LRP robustness, particularly in the  $k = 10$  case: this confirms empirically the conjecture of Section 3.2 that components of the gradient that are normal to the data manifold (and are therefore the ones likely to be changed in an attack) are often major contributors to the relevance in DNN. On the contrary, the Bayesian averaging process greatly reduces the expected relevance of such direction; importantly, we see that this reduction is larger the greater the number of samples, as should be expected.

In Fig. 5 and Fig. 8 in the supplementary material we test the stability of deterministic and Bayesian interpretations w.r.t. FGSM and PGD attacks on 500 test inputs from MNIST. We compute the relevance heatmaps using Gamma, Epsilon and Alpha-Beta rules. The Bayesian networks are trained on MNIST with HMC (Fig. 5) and VI (Fig. 8) and evaluated on 100 samples from the posterior. The experiments confirm that Bayesian explanations are more stable across multiple LRP rules and gradient-based adversarial attacks, also in the internal layers.

## 4.2 Bayesian LRP robustness is correlated with softmax robustness

A simple explanation for the improved LRP robustness of BNNs lies in the fact that BNNs are provably immune to gradient-based attacks [5]. Therefore, one might argue that the stability of the LRP is a trivial byproduct of the stability of the classifications.

To explore this question more in depth, we consider the relationship between the LRP robustness of a test point (stability of the explanation) and its softmax robustness (resilience of the classification against an attack). Fig. 6 and Fig. 10 in the supplementary material show scatterplots of these two quantities for the same models of the previous experiments. An immediate observation is that deterministic explanations are weak against adversarial perturbations even when their softmax robustness (2) is close to 1. Therefore, even in the cases where the classification is unchanged, deterministic saliency heatmaps are fragile. In fact, there are no significant changes in LRP robustness between data points that are vulnerable to attacks and data points that are robust to attacks. Bayesian

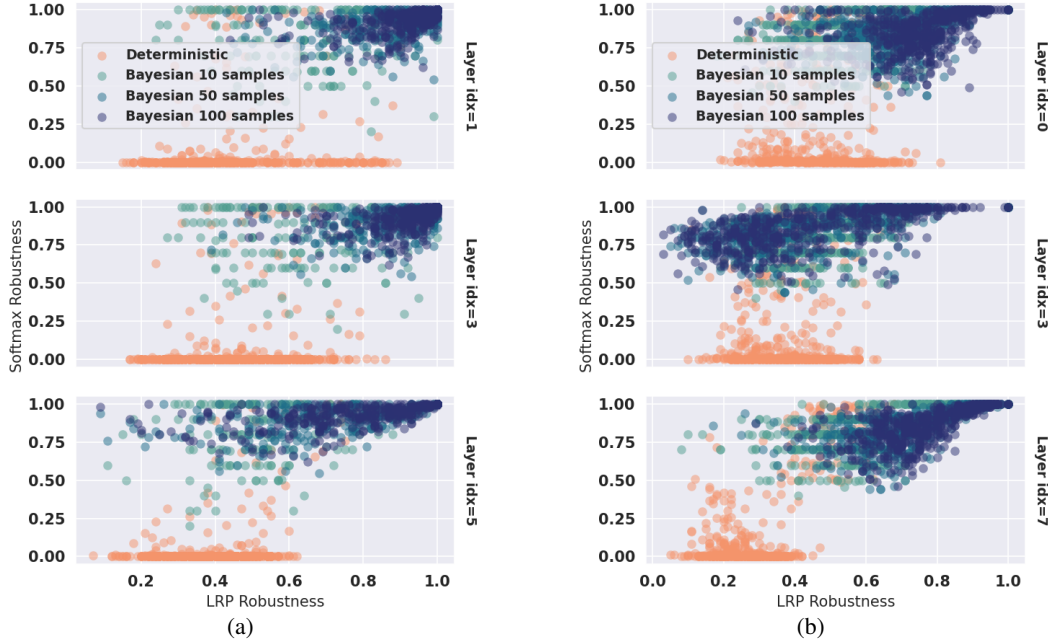


Figure 6: LRP vs Softmax Robustness of deterministic and Bayesian NNs trained on MNIST (a) and Fashion MNIST (b) datasets. LRP Robustness is computed with the Epsilon rule on the 100 most relevant pixels, i.e. using  $\text{Top}_{100}$ . Bayesian Networks are trained with HMC in (a) and VI in (b). Both models are tested with an increasing number of samples (10, 50, 100). Layer indexes refer to the learnable layers in the architectures: fully connected (Tab. 2 in the Appendix) for (a), convolutional (Tab. 1 in the Appendix) for (b).

models, instead, show a strong positive correlation between LRP and softmax robustness, especially as the number of posterior samples increases. While it is immediately evident that Bayesian predictions are robust to adversarial attacks (since most data points have softmax robustness greater than 0.5), it is also clear from this correlation that attacks which are more successful (i.e. lower softmax robustness) also alter more substantially the interpretation of the classification, and are therefore likely to represent genuine directions of change of the true underlying decision function along the data manifold.

## 5 Conclusions

Deep neural networks are fundamental to modern AI, yet many of the mathematical structures underlying their success are still poorly understood. Unfortunately, an unavoidable consequence of this situation is that we also lack principled tools to address the weaknesses of deep learning systems.

In this paper, we harness the geometric perspective to adversarial attacks introduced in [5] to study the resilience of Layer-wise Relevance Propagation heatmaps to adversarial attacks. The geometric analysis suggests a fundamental link between the fragility of DNNs against adversarial attacks and the difficulties in understanding their predictions: because of the unconstrained nature of classifiers defined on high dimensional input spaces but trained on low dimensional data, gradients of both the loss function and the prediction function tend to be dominated by directions which are orthogonal to the data manifold. These directions both give rise to adversarial attacks, and provide spurious explanations which are orthogonal to the natural parametrisation of the data manifold. As shown in [5], a Bayesian treatment should, in the limit of infinite data, remedy the situation by averaging out irrelevant gradient directions in expectation. Not only BNN interpretations are considerably more robust than deterministic DNN, but we also observe a correlation between softmax (adversarial) robustness and LRP robustness which suggests that indeed Bayesian interpretations capture relevant parametrisations of the data manifold.

We point out the presence of theoretical and practical limitations. The strong assumptions in Theorem 3.1, which restrict the geometrical considerations to fully trained BNNs in the limit of an infinite amount of weights and training data, do not prevent us from observing the desired behavior on single channel datasets, i.e. MNIST and Fashion MNIST, even when using cheap approximate inference techniques (VI). However, learning accurate BNNs on more complex datasets (e.g. 3-channels images) is extremely challenging, which makes the Bayesian scheme currently not suitable for large-scale applications. Preliminary experiments on 3-channels images from CIFAR-10 with a ResNet architecture (Fig. 9 in the Appendix) show only a marginal improvement in adversarial and LRP robustness. The causes of such a weakness of deeper BNNs are still unclear, though they may be the effect of a bad approximation of their posterior. This suggests the need for further investigations on such matters, especially on sufficiently accurate and scalable approximate inference methods for BNNs such applications [26].

Nevertheless, we believe that the insights provided by a geometric interpretation will be helpful towards a better understanding of both the strengths and the weaknesses of deep learning.

## References

- [1] David Alvarez-Melis and Tommi S Jaakkola. Towards robust interpretability with self-explaining neural networks. *arXiv preprint arXiv:1806.07538*, 2018.
- [2] Christopher Anders, Plamen Pasliev, Ann-Kathrin Dombrowski, Klaus-Robert Müller, and Pan Kessel. Fairwashing explanations with off-manifold detergent. In *International Conference on Machine Learning*, pages 314–323. PMLR, 2020.
- [3] Sebastian Bach, Alexander Binder, Grégoire Montavon, Frederick Klauschen, Klaus-Robert Müller, and Wojciech Samek. On pixel-wise explanations for non-linear classifier decisions by layer-wise relevance propagation. *PloS one*, 10(7):e0130140, 2015.
- [4] Kirill Bykov, Marina M-C Höhne, Klaus-Robert Müller, Shinichi Nakajima, and Marius Kloft. How much can i trust you?—quantifying uncertainties in explaining neural networks. *arXiv preprint arXiv:2006.09000*, 2020.
- [5] Ginevra Carbone, Matthew Wicker, Luca Laurenti, Andrea Patane, Luca Bortolussi, and Guido Sanguinetti. Robustness of bayesian neural networks to gradient-based attacks. In H. Larochelle, M. Ranzato, R. Hadsell, M. F. Balcan, and H. Lin, editors, *Advances in Neural Information Processing Systems*, volume 33, pages 15602–15613. Curran Associates, Inc., 2020.
- [6] J. Deng, W. Dong, R. Socher, L.-J. Li, K. Li, and L. Fei-Fei. ImageNet: A Large-Scale Hierarchical Image Database. In *CVPR09*, 2009.
- [7] Ann-Kathrin Dombrowski, Maximilian Alber, Christopher J Anders, Marcel Ackermann, Klaus-Robert Müller, and Pan Kessel. Explanations can be manipulated and geometry is to blame. *arXiv preprint arXiv:1906.07983*, 2019.
- [8] Simon Du, Jason Lee, Haochuan Li, Liwei Wang, and Xiyu Zhai. Gradient descent finds global minima of deep neural networks. In *International Conference on Machine Learning*, pages 1675–1685. PMLR, 2019.
- [9] Yarin Gal and Zoubin Ghahramani. Dropout as a bayesian approximation: Representing model uncertainty in deep learning. In *international conference on machine learning*, pages 1050–1059. PMLR, 2016.
- [10] Amirata Ghorbani, Abubakar Abid, and James Zou. Interpretation of neural networks is fragile. In *Proceedings of the AAAI Conference on Artificial Intelligence*, volume 33, pages 3681–3688, 2019.
- [11] Ian Goodfellow, Jonathon Shlens, and Christian Szegedy. Explaining and harnessing adversarial examples. *International Conference on Learning Representations*, 2015.
- [12] Juyeon Heo, Sunghwan Joo, and Taesup Moon. Fooling neural network interpretations via adversarial model manipulation. *arXiv preprint arXiv:1902.02041*, 2019.

- [13] Pieter-Jan Kindermans, Sara Hooker, Julius Adebayo, Maximilian Alber, Kristof T Schütt, Sven Dähne, Dumitru Erhan, and Been Kim. The (un)reliability of saliency methods. In *Explainable AI: Interpreting, Explaining and Visualizing Deep Learning*, pages 267–280. Springer, 2019.
- [14] Ranganath Krishnan and Piero Esposito. Bayesian-torch: Bayesian neural network layers for uncertainty estimation. <https://github.com/IntelLabs/bayesian-torch>, 2020.
- [15] Alex Krizhevsky, Vinod Nair, and Geoffrey Hinton. Cifar-10 (canadian institute for advanced research).
- [16] Alexey Kurakin, Ian J. Goodfellow, and Samy Bengio. Adversarial examples in the physical world. *CoRR*, abs/1607.02533, 2016.
- [17] Yann LeCun and Corinna Cortes. MNIST handwritten digit database. 2010.
- [18] JM Lee. Introduction to smooth manifolds (springer, 2012). 2012.
- [19] Song Mei, Andrea Montanari, and Phan-Minh Nguyen. A mean field view of the landscape of two-layer neural networks. *Proceedings of the National Academy of Sciences*, 115(33):E7665–E7671, 2018.
- [20] Grégoire Montavon, Alexander Binder, Sebastian Lapuschkin, Wojciech Samek, and Klaus-Robert Müller. Layer-wise relevance propagation: an overview. *Explainable AI: interpreting, explaining and visualizing deep learning*, pages 193–209, 2019.
- [21] Grégoire Montavon, Sebastian Lapuschkin, Alexander Binder, Wojciech Samek, and Klaus-Robert Müller. Explaining nonlinear classification decisions with deep taylor decomposition. *Pattern Recognition*, 65:211–222, 2017.
- [22] Radford M Neal et al. Mcmc using hamiltonian dynamics. *Handbook of markov chain monte carlo*, 2(11):2, 2011.
- [23] Grant M Rotskoff and Eric Vanden-Eijnden. Neural networks as interacting particle systems: Asymptotic convexity of the loss landscape and universal scaling of the approximation error. *stat*, 1050:22, 2018.
- [24] Lewis Smith and Yarin Gal. Understanding measures of uncertainty for adversarial example detection. *arXiv preprint arXiv:1803.08533*, 2018.
- [25] Martin J Wainwright and Michael Irwin Jordan. *Graphical models, exponential families, and variational inference*. Now Publishers Inc, 2008.
- [26] Florian Wenzel, Kevin Roth, Bastiaan S Veeling, Jakub Świątkowski, Linh Tran, Stephan Mandt, Jasper Snoek, Tim Salimans, Rodolphe Jenatton, and Sebastian Nowozin. How good is the bayes posterior in deep neural networks really? *arXiv preprint arXiv:2002.02405*, 2020.
- [27] Han Xiao, Kashif Rasul, and Roland Vollgraf. Fashion-mnist: a novel image dataset for benchmarking machine learning algorithms. *arXiv preprint arXiv:1708.07747*, 2017.
- [28] Xinyang Zhang, Ningfei Wang, Hua Shen, Shouling Ji, Xiapu Luo, and Ting Wang. Interpretable deep learning under fire. In *29th {USENIX} Security Symposium ({USENIX} Security 20)*, 2020.

## A Appendix

### A.1 Theoretical results

In the following, we summarize the main background material needed for proving Theorem 3.1.

Theorem 1 in [2] is a generalization of the submanifold extension lemma (e.g. Lemma 5.34 in [18]). It proves that any function  $g$  defined on a submanifold  $\mathcal{M}$  can be extended to an embedding manifold  $\mathcal{R}$ , in such a way that the choice of the derivatives orthogonal to the submanifold is arbitrary. We change the original notation and report it here as Lemma A.1.

**Lemma A.1.** *Let  $\mathcal{M} \subset \mathcal{R}$  be a  $k$ -dimensional submanifold embedded in the  $d$ -dimensional manifold  $\mathcal{R}$ . Let  $V = \sum_{i=k+1}^d v^i \partial_i$  be a conservative vector field along  $\mathcal{M}$  which assigns a vector in  $T_x \mathcal{M}^\perp$  for each  $x \in \mathcal{M}$ . For any smooth function  $g : \mathcal{M} \rightarrow \mathbb{R}$  there exists a smooth extension  $F : \mathcal{R} \rightarrow \mathbb{R}$  such that*

$$F|_{\mathcal{M}} = g,$$

where  $F|_{\mathcal{M}}$  denotes the restriction of  $F$  on the submanifold  $\mathcal{M}$ , and s.t. the derivative of the extension  $F$  is

$$\nabla_x F(x) = (\nabla_1 g(x), \dots, \nabla_k g(x), v^{k+1}(x), \dots, v^d(x))$$

for all  $x \in \mathcal{M}$ .

We use Lemma A.1 in Corollary A.1 to build an extension of the prediction function outside of the data manifold, with suitable derivatives in the orthogonal components.

In the proof of Corollary A.1 we also leverage results on the global convergence of over-parametrised neural networks [8, 19, 23] to approximate the extension of the prediction function with an infinitely wide neural network. Here we report the Universal Representation Theorem from [23] as Lemma A.2, in the limit of infinite training data and infinite number of neurons/ weights (overparametrized network). In doing so, we refer to the notation in Sec. 7 of [5].

**Lemma A.2.** *Let  $f(x, w)$  be a neural network with differentiable and discriminating units, whose weights are drawn from a measure  $\mu(w)$ . Let  $\tilde{f}(x)$  be a target function observed at points drawn from a data distribution  $p(D)$  with support  $\mathcal{M}_D \subset \mathbb{R}^d$ . Suppose that:*

- The input and feature spaces of  $f$  are closed Riemannian manifolds.
- The data distribution  $p(D)$  is non degenerate.

*Then, the training loss function is a convex functional of the measure in the space of weights. Moreover, in the infinite data and overparametrized limit, stochastic gradient descent converges to the global minimum  $\tilde{f}(x)$ , i.e. the loss function is null on the data manifold  $\mathcal{M}_D$ .*

Using Lemma A.1 and Lemma A.2, we can prove that it is always possible to select two sets of weights,  $w$  and  $w'$ , such that the orthogonal gradients of the prediction function at a point  $x$  on the data manifold are opposite.

**Corollary A.1.** *Let  $\mathcal{M}_D \subset \mathbb{R}^d$  be an a.e. smooth manifold and let  $f(x, w)$  be an infinitely wide Bayesian neural network, at full convergence of the training algorithm on  $\mathcal{M}_D$ . For any choice of weights  $w$  and  $x \in \mathcal{M}_D$  there exists a set of weights  $w'$  such that  $f(\cdot, w)|_{\mathcal{M}_D} = f(\cdot, w')|_{\mathcal{M}_D}$  and*

$$\nabla_x^\perp f(x, w) = -\nabla_x^\perp f(x, w'). \quad (6)$$

*Proof.* Let  $F : \mathbb{R}^d \rightarrow \mathbb{R}$  be a smooth function s.t.  $F = f(\cdot, w)$ . From A.1 we know that there exists a smooth extension  $F'$  of  $F|_{\mathcal{M}_D}$  to the embedding space  $\mathbb{R}^d$  such that  $\nabla_x^\perp F'(x) = -\nabla_x^\perp f(x)$ . Moreover, Lemma A.2 holds for  $f$  in the limit of infinite weights, thus there exists a set of weights  $w'$  such that  $f(\cdot, w') = F'$ . This proves equation 6.  $\square$

*Proof of Theorem 3.1.* As a direct consequence of Corollary A.1, under the assumption that the prior distribution  $p(w)$  is uninformative, for any choice of weights such that the loss is zero on the data manifold, we obtain the same likelihood function and the same posterior distribution  $p(w|D)$ . This in

particular holds for any pair  $w, w'$  constructed according to Corollary A.1. Therefore, the orthogonal gradient of the prediction function evaluated on any  $x \in \mathcal{M}_D$  vanishes in expectation, i.e.

$$\mathbb{E}_{p(w|D)} [\nabla_x^\perp f(x, w)] = 0.$$

□

## A.2 LRP Rules

A practical example of propagation rule is the *Epsilon rule* ( $\epsilon$ -LRP) [20]. Let  $a_j$  be a neuron activation computed at the  $j$ -th layer during the forward pass. Let  $w_{jk}$  be the weight connecting  $a_j$  to a subsequent neuron  $a_k$ ,  $w_{0k}$  be the bias weight and  $a_0 = 1$ . At each step of backpropagation LRP computes the relevance score  $R_j$  of the  $j$ -th activation  $a_j$ , by backpropagating the relevance scores of all neurons in the subsequent layer. The resulting  $\epsilon$ -LRP score for a chosen  $\epsilon > 0$  amounts to

$$R_j = \sum_k \frac{a_j w_{jk}}{\epsilon + \sum_{0,j} a_j w_{jk}} R_k. \quad (7)$$

The *Gamma rule* ( $\gamma$ -LRP) favours positive contributions over negative contributions by a factor of  $\gamma$ . The score for a chosen  $\gamma > 0$  is

$$R_j = \sum_k \frac{a_j \cdot (w_{jk} + \gamma \max(0, w_{jk}))}{\sum_{0,j} a_j \cdot (w_{jk} + \gamma \max(0, w_{jk}))} R_k. \quad (8)$$

Finally, the *Alpha-Beta rule* ( $\alpha\beta$ -LRP) computes

$$R_j = \sum_k \left( \alpha \cdot \frac{\max(0, a_j w_{jk})}{\sum_{0,j} \max(0, a_j w_{jk})} - \beta \cdot \frac{\min(0, a_j w_{jk})}{\sum_{0,j} \min(0, a_j w_{jk})} \right) R_k, \quad (9)$$

where the conservative property holds for any choice of  $\alpha$  and  $\beta$  s.t.  $\alpha - \beta = 1$ .

We refer to [20] (Sec 10.2.3) for a complete derivation of the propagation rules listed above within the Deep Taylor Decomposition framework [21]. Notice that for the  $\alpha\beta$ -LRP rule this generalization holds only when  $\alpha = 1$  and  $\beta = 0$ , which are the values used in Fig. 5, 8 and 9.

## A.3 Architectures and Hyperparameters

Table 1: Learnable layers and corresponding indexes in the convolutional architecture. Hidden size is reported in Tab. 3 and Tab. 4.

Idx	Layer	Parameters
0	2D Conv.	<code>in_channels = 784</code> <code>out_channels = 32</code> <code>kernel_size = 5</code>
3	2D Conv.	<code>in_channels = 32</code> <code>out_channels = hidden size</code> <code>kernel_size = 5</code>
7	F.c.	<code>out_features = 10</code>

Table 2: Learnable layers and corresponding indexes in the fully connected architecture. Hidden size is reported in Tab. 3 and Tab. 4.

Idx	Layer	Parameters
1	F. c.	<code>in_features = 784</code> <code>out_features = hidden size</code>
3	F. c.	<code>in_features = hidden size</code> <code>out_features = hidden size</code>
5	F. c.	<code>in_features = hidden size</code> <code>out_features = 10</code>

Table 3: Hyperparameters for BNNs trained with VI.

Dataset	MNIST	Fashion MNIST
Training inputs	60k	60k
Hidden size	512	1024
Nonlinear activations	Leaky ReLU	Leaky ReLU
Architecture	convolutional	convolutional
Training epochs	5	15
Learning rate	0.01	0.001

Table 4: Hyperparameters for BNNs trained with HMC.

Dataset	MNIST	Fashion MNIST
Training inputs	60k	60k
Hidden size	512	1024
Nonlinear activation	Leaky ReLU	Leaky ReLU
Architectures	fully connected	fully connected
Warmup samples	100	100
Numerical integrator stepsize	0.5	0.5
N. steps for numerical integrator	10	10

#### A.4 Additional Experiments

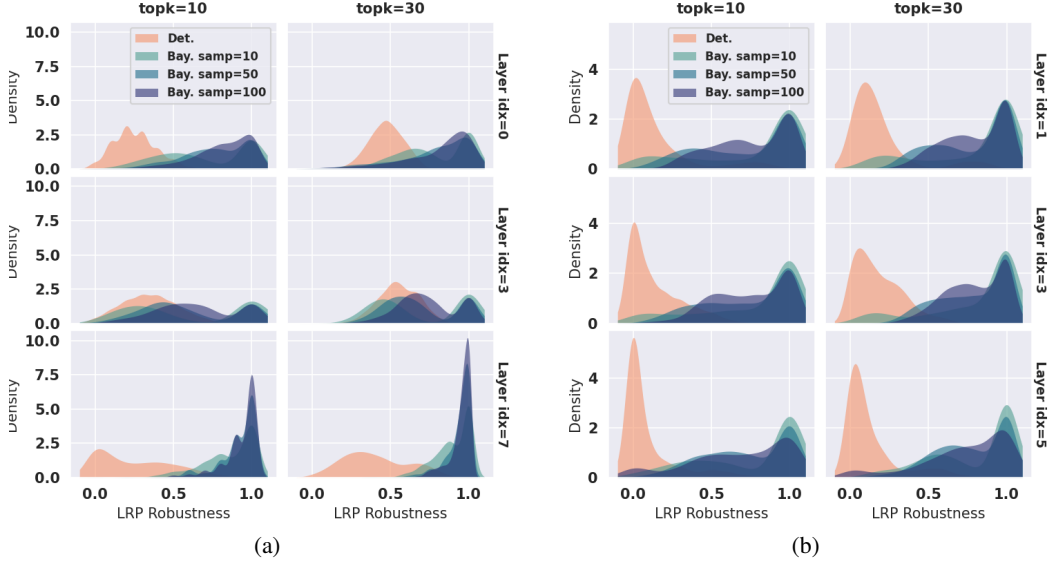


Figure 7: LRP robustness distributions for FGSM attacks computed on 500 test points from MNIST (a) and Fashion MNIST (b) datasets, using the Epsilon rule. Networks in (a) have a convolutional architecture (Tab. 1 in the Appendix) and are trained with VI. Networks in (b) have a fully connected architecture (Tab. 2 in the Appendix) and are trained with HMC. Bayesian networks are tested with an increasing number of samples (10, 50, 100). Layer indexes refer to the learnable layers in the architectures.

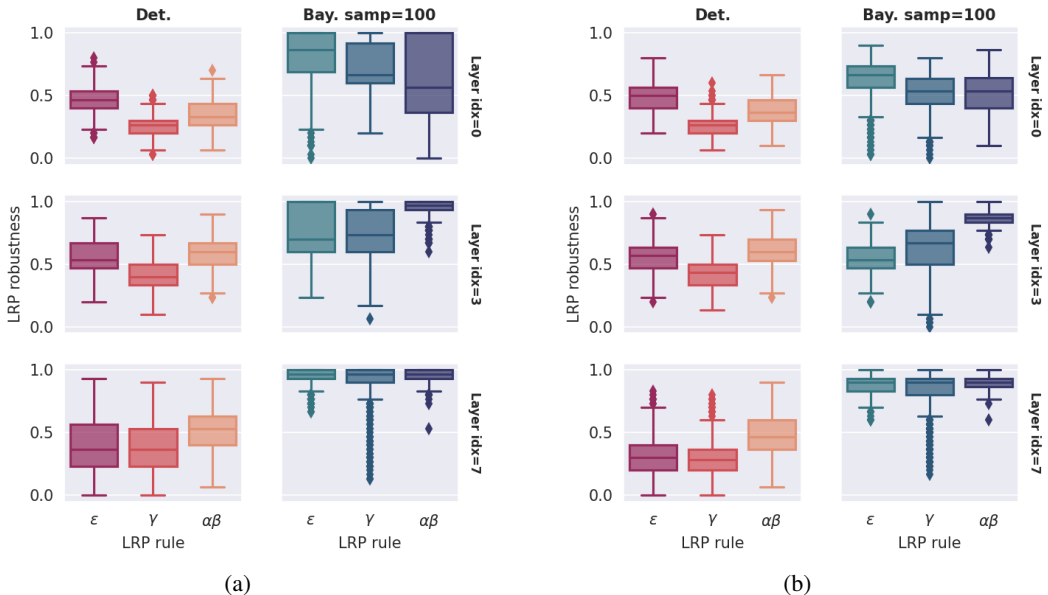


Figure 8: LRP robustness for FGSM (a) and PGD (b) attacks computed on 500 test points from MNIST dataset using Epsilon, Gamma and Alpha-Beta rules on the Top<sub>30</sub> pixels. Deterministic and Bayesian networks have the same convolutional architecture (Tab. 1) and are trained with VI. Layer indexes refer to the learnable layers in the architecture. Bayesian networks are tested with 100 posterior samples. The parameters are set to:  $\epsilon = 0.1$ ,  $\gamma = 0.1$ ,  $\alpha = 1$ ,  $\beta = 0$ .

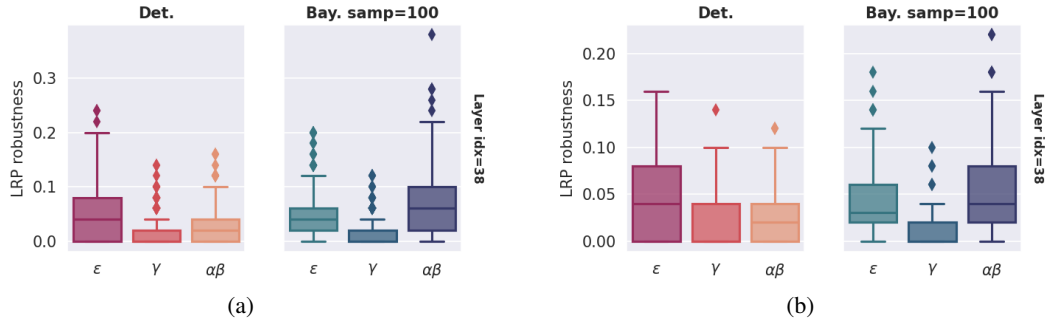


Figure 9: LRP robustness for FGSM (a) and PGD (b) attacks computed on 500 test points from CIFAR-10 dataset using Epsilon, Gamma and Alpha-Beta rules on the Top<sub>50</sub> pixels. Deterministic and Bayesian networks have the same architecture and are trained with VI. Layer indexes refer to the learnable layers in the architecture. Bayesian networks are tested with 100 posterior samples. The parameters are set to:  $\epsilon = 0.1$ ,  $\gamma = 0.1$ ,  $\alpha = 1$ ,  $\beta = 0$ . LRP heatmaps are computed w.r.t. the last layer of a ResNet architecture from `bayesian_torch` [14] library. In this setting, Bayesian and deterministic adversarial accuracies are comparable, suggesting that the approximation induced by VI might be too coarse for a deep architecture. This drop in adversarial robustness has a strong impact on the LRP robustness.

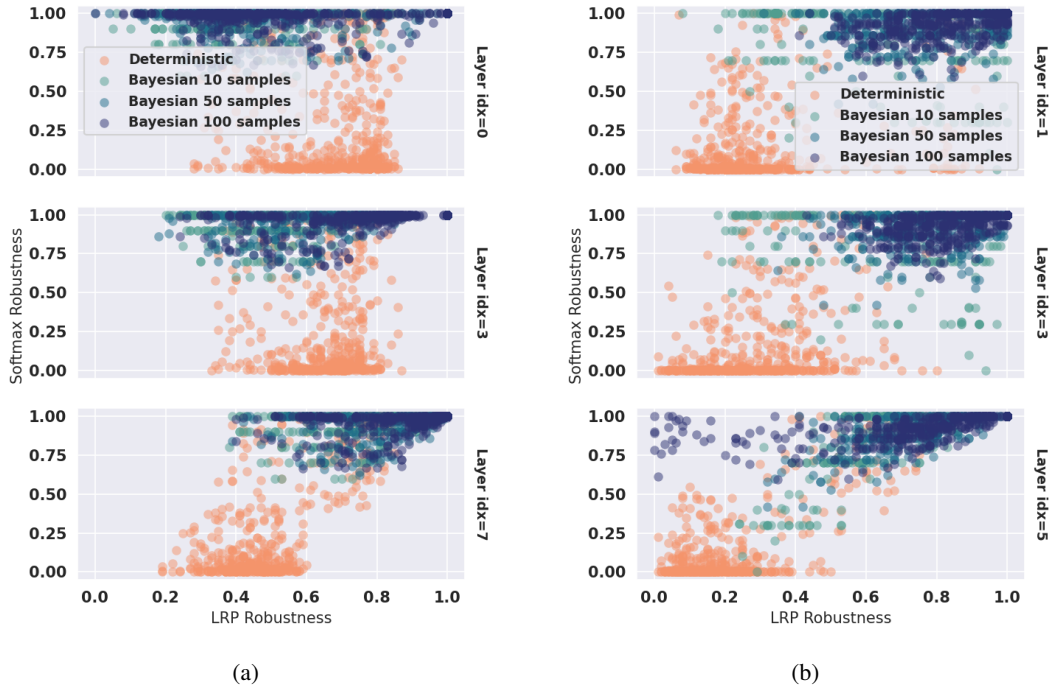


Figure 10: LRP vs Softmax Robustness of deterministic and Bayesian NNs trained on MNIST (a) and Fashion MNIST (b) datasets. LRP Robustness is computed with the Epsilon rule on the 100 most relevant pixels, i.e. using Top<sub>100</sub>. Bayesian Networks are trained with HMC in (a) and VI in (b). Both models are tested with an increasing number of samples (10, 50, 100). Layer indexes refer to the learnable layers in the architectures: convolutional (Tab. 1 in the Appendix) for (a), fully connected (Tab. 2 in the Appendix) for (b).